IOPscience iopscience.iop.org

Home Search Collections Journals About Contact us My IOPscience

Theory of bound magnetic polarons in diluted magnetic semiconductors

This article has been downloaded from IOPscience. Please scroll down to see the full text article.

1989 J. Phys.: Condens. Matter 1 941

(http://iopscience.iop.org/0953-8984/1/5/011)

View the table of contents for this issue, or go to the journal homepage for more

Download details:
IP Address: 171.66.16.90
The article was downloaded on 10/05/2010 at 17:39

Please note that terms and conditions apply.

J. Phys.: Condens. Matter 1 (1989) 941–956. Printed in the UK

Theory of bound magnetic polarons in diluted magnetic semiconductors

U Thibblin†, R Micnas‡ and K A Chao†

† Department of Physics and Measurement Technology, University of Linköping, S-58183 Linköping, Sweden

‡ Institute of Physics, A Mickiewicz University, 60769 Poznan, Poland

Received 19 July 1988

Abstract. A theory of bound magnetic polarons (BMPs) in dilute magnetic semiconductors is formulated by applying the functional integral method (FIM). The effects of the antiferromagnetic Mn–Mn interaction on BMPs in dilute systems such as $Cd_{1-x}Mn_xSe$, $Cd_{1-x}Mn_xTe$, and $Cd_{1-x}Mn_xS$ are included in terms of clusters. Within the framework of the static approximation to the FIM, the spin-flip Raman scattering spectrum and the binding energy of BMPs are calculated. The theoretical results are compared with available experimental data.

1. Introduction

Experiments on dilute magnetic semiconductors suggest the formation of bound magnetic polarons (BMPs) due to the s–d (p–d) exchange interaction between the Mn^{2+} ions and electrons bound to donors (or holes to acceptors). The BMPs in $Cd_{1-x}Mn_xSe$, $Cd_{1-x}Mn_xTe$ and $Cd_{1-x}Mn_xS$ have been extensively studied experimentally with luminescence [1–3] and spin-flip Raman scattering [4–8] measurements. Dietl and Spalek [9, 10] and Dietl [11] used the Ginzburg–Landau theory, and treated the spin fluctuations using the Gaussian approximation, to formulate a theory for BMPs. Later, Swierkowski and Dietl [12] extended the theory beyond the Gaussian approximation. The theory of Heiman and co-workers [7], Wolff and Warnock [13] and Warnock and Wolff [14], assuming a semiclassical Mn^{2+} subsystem, is equivalent to that of Dietl and Spalek in the appropriate limit. Other theoretical investigations of BMPs either used a classical spin picture [3] or a cluster-type calculation [15–18]. The antiferromagnetic Mn–Mn exchange interaction has been taken into account either phenomenologically [3, 7, 9–15] or in the form of clusters [17, 18].

In this paper a detailed version of the functional integral approach to the BMP, published earlier by the same authors [19], is presented, and the theory is also extended to include the antiferromagnetic interaction between the manganese ions, in terms of small clusters. It is shown that existing theories are on the level of the static approximation. It is also demonstrated how we can calculate the spin-flip Raman scattering spectrum with the functional integral method. Except as regards the different ways in which the antiferromagnetic Mn–Mn interaction is included, our results agree with those obtained by Dietl [11], in the appropriate limit. If the Mn–Mn interaction is

0953-8984/89/050941 + 16 $02.50 © 1989 IOP Publishing Ltd

neglected, our results agree with those obtained by Heiman and co-workers [7]. Finally the theoretical results are compared with available experimental data.

2. The BMP partition function

We start from the Golnik-Gaj-Nawrocki-Planel-Benoit (GGNPB) effective-mass Hamiltonian for a BMP [1, 7, 10]:

$$H = p^2/2m^* - e^2/\varepsilon r - J\sum_j \boldsymbol{s}\cdot\boldsymbol{S}_j\delta(\boldsymbol{r}-\boldsymbol{R}_j) \tag{2.1}$$

where ε is the dielectric constant, m^* the effective mass of an electron (or a hole) in the host semiconductor without Mn^{2+} ions, and J the exchange constant. Usually J is written in terms of $N_0\alpha = N_0 J$ for an electron and $N_0\beta = 3N_0 J$ for a hole, where N_0 is the number of cation sites per unit volume. $N_0\alpha$ and $N_0\beta$ can be determined from the experimental data. $\boldsymbol{p}$ and $\boldsymbol{r}$ are variables associated with the electron (or hole), and $\boldsymbol{R}_j$ and $\boldsymbol{S}_j$ are, respectively, the position and spin of the jth Mn^{2+} ion. s is the spin of the electron ($s = \frac{1}{2}$) or the effective spin of the hole ($s = \frac{3}{2}$). The first two terms in (2.1) describe the electron (or hole) bound to a donor (or an acceptor). We assume a wavefunction of the localised electron (or hole) of the form

$$\psi(\boldsymbol{r}) = F(\boldsymbol{r})u_0(\boldsymbol{r}) = \pi^{-1/2}a_B^{-3/2}\exp(-r/a_B)u_0(\boldsymbol{r}) \tag{2.2}$$

where a_B is the effective Bohr radius, and $u_0(\boldsymbol{r})$ is the periodic band-edge Bloch function. In this paper we will restrict ourselves to systems with low Mn concentration. Therefore we will neglect the effect of Mn^{2+} ions on the wavefunction (2.2). With these simplifications one can use a Hartree-type function [7, 10]

$$\bar{\psi}(\boldsymbol{r}, s; \{\boldsymbol{S}_j\}) \simeq F(\boldsymbol{r})\chi(s, \{\boldsymbol{S}_j\}) \tag{2.3}$$

for the whole system and rewrite the Hamiltonian as

$$H = E(a) + H_{BMP} \tag{2.4}$$

where $E(a) = h^2/2m^*a^2 - e^2/\varepsilon a$ is the usual donor (or acceptor) energy. If we now introduce the interaction between the Mn^{2+} ions and an external magnetic field $\boldsymbol{B}_0$, the spin Hamiltonian for the BMP can be written as

$$H_{BMP} = H_0 + H_1 \tag{2.5}$$

where

$$H_0 = -\boldsymbol{b}_1\cdot\boldsymbol{s} - \boldsymbol{b}_2\cdot\sum_j \boldsymbol{S}_j - \sum_{i,j} I_{ij}\boldsymbol{S}_i\cdot\boldsymbol{S}_j \tag{2.6}$$

and

$$H_1 = -\boldsymbol{s}\cdot\boldsymbol{\Gamma}, \tag{2.7}$$

with the definitions $\boldsymbol{b}_1 = g^*\mu_B\boldsymbol{B}_0$, $\boldsymbol{b}_2 = g_{Mn}\mu_B\boldsymbol{B}_0$, and $\boldsymbol{\Gamma} = \Sigma_j K_j\boldsymbol{S}_j$ where $K_j = J|F(\boldsymbol{R}_j)|^2$. In (2.6), g^* is the electron (or hole) g-factor in the host semiconductor without Mn^{2+} ions, and g_{Mn} is the g-factor of an isolated Mn^{2+} ion. The last term in (2.6) describes the interaction between the Mn^{2+} ions, with I_{ij} being the exchange parameter.

We need to calculate the partition function for a given distribution of Mn^{2+} ions in

the host semiconductor.

$$Z_{\mathrm{BMP}} = \mathrm{Tr}[\exp(-\beta H_0 - \beta H_1)] \tag{2.8}$$

Since the operators H_0 and H_1 do not commute, we write [20]

$$Z_{\mathrm{BMP}} = \mathrm{Tr}\left\{\exp(-\beta H_0) T_\tau \left[\exp\left(-\int_0^\beta H_1(\tau)\,\mathrm{d}\tau\right)\right]\right\} \tag{2.9}$$

where $H_1(\tau) = \exp(\tau H_0) H_1 \exp(-\tau H_0)$, and T_τ is the ordering operator with respect to the Matsubara time τ.

We follow the standard procedure [21–23] to construct the functional integral representation of (2.9). The interval $[0, \tau]$ is divided into M steps $\tau_n = \beta n/M$ with $n = 0, 1, \ldots, M$, and for each τ_n we apply the generalised Hubbard–Stratonovich identity for two commuting operators A and B:

$$\exp(AB) = \frac{1}{\pi}\int_{-\infty}^{\infty} \mathrm{d}x \int_{-\infty}^{\infty} \mathrm{d}y \exp[-(x^2 + y^2) + (A + B)x + \mathrm{i}(A - B)y]. \tag{2.10}$$

Then (2.10) becomes

$$\begin{aligned} Z_{\mathrm{BMP}} = \mathrm{Tr}\Bigg[& \exp(-\beta H_0) \lim_{M\to\infty} T_\tau \int_{-\infty}^{\infty} \prod_{n=1}^{M} (\pi M)^{-3/2}\,\mathrm{d}\boldsymbol{x}_n \int_{-\infty}^{\infty} \prod_{n=1}^{M} (\pi M)^{-3/2}\,\mathrm{d}\boldsymbol{y}_n \\ & \times \exp\left(\frac{1}{M}\sum_{n=1}^{M}(x_n^2 + y_n^2)\right) \exp\left(\frac{\sqrt{\beta}}{M}\sum_{n=1}^{M}(\boldsymbol{\Gamma}(\tau_n) + \boldsymbol{s}(\tau_n))\cdot\boldsymbol{x}_n\right) \\ & \times \exp\left(\frac{\mathrm{i}\sqrt{\beta}}{M}\sum_{n=1}^{M}(\boldsymbol{\Gamma}(\tau_n) - \boldsymbol{s}(\tau_n))\cdot\boldsymbol{y}_n\right)\Bigg] \end{aligned} \tag{2.11}$$

where $\boldsymbol{x}_n$ and $\boldsymbol{y}_n$ are two auxiliary vector fields. In the limit $M \to \infty$, $\boldsymbol{x}_n$ and $\boldsymbol{y}_n$ become two continuous functions $\boldsymbol{x}(\tau)$ and $\boldsymbol{y}(\tau)$ in the interval $[0, \beta]$ with the boundary conditions $\boldsymbol{x}(0) = \boldsymbol{x}(\beta)$ and $\boldsymbol{y}(0) = \boldsymbol{y}(\beta)$. Let us define the measure

$$\int \mathrm{D}\boldsymbol{x} \int \mathrm{D}\boldsymbol{y} \ldots \equiv \lim_{M\to\infty} \int_{-\infty}^{\infty} \prod_{n=1}^{M} (\pi M)^{-3/2}\,\mathrm{d}\boldsymbol{x}_n \int_{-\infty}^{\infty} \prod_{n=1}^{M} (\pi M)^{-3/2}\,\mathrm{d}\boldsymbol{y}_n \ldots. \tag{2.12}$$

We then arrive at the exact partition function

$$Z_{\mathrm{BMP}} = Z_0 \int \mathrm{D}\boldsymbol{x} \int \mathrm{D}\boldsymbol{y} \exp(-\varphi[\boldsymbol{x}, \boldsymbol{y}]) \tag{2.13}$$

where $Z_0 = \mathrm{Tr}[\exp(-\beta H_0)]$ and

$$\begin{aligned} \varphi[\boldsymbol{x}, \boldsymbol{y}] = \frac{1}{\beta}\int_0^\beta \{\boldsymbol{x}(\tau)^2 + \boldsymbol{y}(\tau)^2\}\,\mathrm{d}\tau - \ln\Bigg\langle T_\tau\Bigg[\exp\Bigg(\beta^{-1/2} \\ \times \int_0^\beta \mathrm{d}\tau[\boldsymbol{\Gamma}(\tau)\cdot(\boldsymbol{x}(\tau) + \mathrm{i}\boldsymbol{y}(\tau)) + \boldsymbol{s}(\tau)\cdot(\boldsymbol{x}(\tau) - \mathrm{i}\boldsymbol{y}(\tau))]\Bigg)\Bigg]\Bigg\rangle_0. \end{aligned} \tag{2.14}$$

The thermodynamic average is defined as

$$\langle \ldots \rangle_0 = \mathrm{Tr}[\exp(-\beta H_0) \ldots]/Z_0. \tag{2.15}$$

We now split the auxiliary fields as follows:

$$x(\tau) = x_0 + x_f(\tau) \qquad y(\tau) = y_0 + y_f(\tau)$$

where

$$x_0 = \frac{1}{\beta}\int_0^\beta x(\tau)\,d\tau \qquad y_0 = \frac{1}{\beta}\int_0^\beta y(\tau)\,d\tau.$$

If we define

$$Z_{st}(x_0, y_0) = \mathrm{Tr}[\exp(-\beta H_{st})] \tag{2.16}$$

where

$$H_{st} = H_0 - \beta^{-1/2}[\Gamma\cdot(x_0 + iy_0) + s\cdot(x_0 - iy_0)] \tag{2.17}$$

equation (2.14) can be rewritten as

$$Z_{BMP} = \int_{-\infty}^{\infty} \pi^{-3/2}\,dx_0 \int_{-\infty}^{\infty} \pi^{-3/2}\,dy_0 \exp(-x_0^2 - y_0^2) Z_{st}(x_0, y_0)$$
$$\times \int Dx_f \int Dy_f \exp(-\varphi[x_f, y_f]) \tag{2.18}$$

where

$$\varphi[x_f, y_f] = \frac{1}{\beta}\int_0^\beta (x_f^2(\tau) + y_f^2(\tau))\,d\tau - \ln\left\langle T_\tau\left[\exp\left(\beta^{-1/2}\right.\right.\right.$$
$$\left.\left.\left.\times \int_0^\beta d\tau[\Gamma_f(\tau)\cdot(x_f(\tau) + iy_f(\tau)) + s_f(\tau)\cdot(x_f(\tau) - iy_f(\tau))]\right)\right]\right\rangle_{st} \tag{2.19}$$

and $\Gamma_f(\tau)$ and $s_f(\tau)$ are in the Heisenberg representation with respect to H_{st}. It is difficult to calculate Z_{BMP} from (2.18), so to continue our analysis we will neglect the time-dependent parts $x_f(\tau)$ and $y_f(\tau)$, and keep only the static parts x_0 and y_0 of (2.18). This is the static approximation which accounts for the thermodynamic fluctuations but neglects most of the quantum fluctuations.

$$\tilde{Z}_{BMP} = \int_{-\infty}^{\infty} \pi^{-3/2}\,dx_0 \int_{-\infty}^{\infty} \pi^{-3/2}\,dy_0\, Z_{st}(x_0, y_0). \tag{2.20}$$

Before going further, let us point out that for pure Ising coupling and with $H_0 = 0$, the static approximation yields the exact result

$$\tilde{Z}_{BMP} = \prod_{j=1}^{N} \frac{2\sinh[(s + \frac{1}{2})(\beta/2)K_j]}{\sinh[(\beta/4)K_j]}. \tag{2.21}$$

By introducing the new variables $\lambda = i\sqrt{\beta}(x_0 + iy_0)$ and $\gamma = (x_0 - iy_0)/\sqrt{\beta}$ equation (2.20) can be written as

$$\tilde{Z}_{BMP} = (2\pi)^{-3} \int_{-\infty}^{\infty} d\lambda \int_{-\infty}^{\infty} d\gamma \exp(i\lambda\cdot\gamma)$$
$$\times \mathrm{Tr}\{\exp[-\beta(H_0 + i\Gamma\cdot\lambda/\beta - s\cdot\gamma)]\}. \tag{2.22}$$

If we neglect the exchange interaction between the Mn^{2+} ions, that is we put I_{ij} equal to

zero, then (2.22) reduces to the formula proposed by Wolff and co-workers [7, 13, 14] in their spherical model on BMPs, which treats the Mn^{2+} spins semiclassically.

If in (2.22) we take the trace over the electron (or hole) spin and introduce the new variable $\boldsymbol{\Delta} = \boldsymbol{\gamma} + \boldsymbol{b}_1$, we then have

$$\tilde{Z}_{\mathrm{BMP}} = (2\pi)^{-3} \int_{-\infty}^{\infty} \mathrm{d}\boldsymbol{\Delta} \int_{-\infty}^{\infty} \mathrm{d}\boldsymbol{\lambda} \exp[\mathrm{i}\boldsymbol{\lambda} \cdot (\boldsymbol{\Delta} - \boldsymbol{b}_1)] f(\beta\Delta) Z_{\mathrm{Mn}} \tag{2.23}$$

where

$$f(\beta\Delta) = 2\cosh(\beta\Delta/2) \tag{2.24}$$

for an electron, and

$$f(\beta\Delta) = 2\cosh(3\beta\Delta/2) + 2\cosh(\beta\Delta/2) \tag{2.25}$$

for a hole, and

$$Z_{\mathrm{Mn}} = \mathrm{Tr}_{\{S_j\}} \exp[-\beta(\tilde{H}_0 + \tilde{H}_1)] \tag{2.26}$$

where

$$\tilde{H}_0 = -\boldsymbol{b}_2 \cdot \sum_j \boldsymbol{S}_j - \sum_{i,j} I_{ij} \boldsymbol{S}_i \cdot \boldsymbol{S}_j \tag{2.27}$$

and

$$\tilde{H}_1 = \frac{\mathrm{i}}{\beta} \boldsymbol{\lambda} \cdot \sum_j K_j \boldsymbol{S}_j. \tag{2.28}$$

Since we consider systems with low Mn^{2+} concentration we will divide the Mn^{2+} subsystem into isolated (i) Mn^{2+}, pairs (p), open triangles (t) and closed triangles (c) of Mn^{2+}, and we will only take nearest-neighbour interactions into account. Furthermore, we let the external magnetic field be along the z axis, $\boldsymbol{B}_0 = (0, 0, B_0)$. $\tilde{H}_0$ then takes the form

$$H_0 = \sum_{\mathrm{i}} H_{\mathrm{i}}^0 + \sum_{\mathrm{p}} H_{\mathrm{p}}^0 + \sum_{\mathrm{t}} H_{\mathrm{t}}^0 + \sum_{\mathrm{c}} H_{\mathrm{c}}^0, \tag{2.29}$$

where

$$H_{\mathrm{i}}^0 = -b_2 S_{\mathrm{i}}^z \tag{2.30a}$$

$$H_{\mathrm{p}}^0 = -b_2(S_{\mathrm{p1}}^z + S_{\mathrm{p2}}^z) - 2I\boldsymbol{S}_{\mathrm{p1}} \cdot \boldsymbol{S}_{\mathrm{p2}} \tag{2.30b}$$

$$H_{\mathrm{t}}^0 = -b_2(S_{\mathrm{t1}}^z + S_{\mathrm{t2}}^z + S_{\mathrm{t3}}^z) - 2I(\boldsymbol{S}_{\mathrm{t1}} \cdot \boldsymbol{S}_{\mathrm{t2}} + \boldsymbol{S}_{\mathrm{t2}} \cdot \boldsymbol{S}_{\mathrm{t3}}) \tag{2.30c}$$

and

$$H_{\mathrm{c}}^0 = -b_2(S_{\mathrm{c1}}^z + S_{\mathrm{c2}}^z + S_{\mathrm{c3}}^z) - 2I(\boldsymbol{S}_{\mathrm{c1}} \cdot \boldsymbol{S}_{\mathrm{c2}} + \boldsymbol{S}_{\mathrm{c2}} \cdot \boldsymbol{S}_{\mathrm{c3}} + \boldsymbol{S}_{\mathrm{c3}} \cdot \boldsymbol{S}_{\mathrm{c1}}) \tag{2.30d}$$

where I denotes the nearest-neighbour exchange integral. The eigenvalues of (2.30*a*)–(2.30*d*) can easily be calculated and are shown in Appendix 1. $\tilde{H}_1$ takes the form

$$\tilde{H}_1 = \frac{\mathrm{i}}{\beta} \boldsymbol{\lambda} \cdot \Big(\sum_{\mathrm{i}} K_{\mathrm{i}} \boldsymbol{S}_{\mathrm{i}} + \sum_{p} (K_{\mathrm{p1}} \boldsymbol{S}_{\mathrm{p1}} + K_{\mathrm{p2}} \boldsymbol{S}_{\mathrm{p2}}) + \sum_{\mathrm{t}} (K_{\mathrm{t1}} \boldsymbol{S}_{\mathrm{t1}} + K_{\mathrm{t2}} \boldsymbol{S}_{\mathrm{t2}} + K_{\mathrm{t3}} \boldsymbol{S}_{\mathrm{t3}}) + \sum_{\mathrm{c}} (K_{\mathrm{c1}} \boldsymbol{S}_{\mathrm{c1}} + K_{\mathrm{c2}} \boldsymbol{S}_{\mathrm{c2}} + K_{\mathrm{c3}} \boldsymbol{S}_{\mathrm{c3}}) \Big). \tag{2.31}$$

If we use an average distance between the donor (or the acceptor) and a cluster, $\tilde{H}_1$ can be written as

$$\tilde{H}_1 = \frac{\mathrm{i}}{\beta}\boldsymbol{\lambda}\cdot\left(\sum_{\mathrm{i}} K_{\mathrm{i}}\boldsymbol{S}_{\mathrm{i}} + \sum_{\mathrm{p}} K_{\mathrm{p}}\boldsymbol{S}_{\mathrm{p}} + \sum_{\mathrm{t}} K_{\mathrm{t}}\boldsymbol{S}_{\mathrm{t}} + \sum_{\mathrm{c}} K_{\mathrm{c}}\boldsymbol{S}_{\mathrm{c}}\right) \tag{2.32}$$

where $\boldsymbol{S}_{\mathrm{p}} = \boldsymbol{S}_{\mathrm{p1}} + \boldsymbol{S}_{\mathrm{p2}}, \boldsymbol{S}_{\mathrm{t}} = \boldsymbol{S}_{\mathrm{t1}} + \boldsymbol{S}_{\mathrm{t2}} + \boldsymbol{S}_{\mathrm{t3}}$ and $\boldsymbol{S}_{\mathrm{c}} = \boldsymbol{S}_{\mathrm{c1}} + \boldsymbol{S}_{\mathrm{c2}} + \boldsymbol{S}_{\mathrm{c3}}$. The calculation should not be sensitive to this approximation for the small clusters we are considering; however, if we include the interaction between more distant Mn^{2+} ions, this approximation needs to be improved.

Since $\tilde{H}_0$ and $\tilde{H}_1$ do not commute, we write (2.26) as

$$Z_{\mathrm{Mn}} = \mathrm{Tr}_{\{S_j\}}\left[\exp(-\beta\tilde{H}_0)T_\tau \exp\left(-\int_0^\beta \tilde{H}_1(\tau)\,\mathrm{d}\tau\right)\right] \tag{2.33}$$

and calculate it with the cumulant expansion. To the second order, we have

$$\begin{aligned} Z_{\mathrm{Mn}} = \tilde{Z}_0 \exp\Bigg[&-\mathrm{i}\left(\langle S_{\mathrm{i}}^z\rangle_0 \sum_{\mathrm{i}} K_{\mathrm{i}} + \langle S_{\mathrm{p}}^z\rangle_0 \sum_{\mathrm{p}} K_{\mathrm{p}} + \langle S_{\mathrm{t}}^z\rangle_0 \sum_{\mathrm{t}} K_{\mathrm{t}} + \langle S_{\mathrm{c}}^z\rangle_0 \sum_{\mathrm{c}} K_{\mathrm{c}}\right)\lambda_z \\ &-\frac{1}{2\beta}\left(\chi_1^{\parallel}\sum_{\mathrm{i}} K_{\mathrm{i}}^2 + \chi_2^{\parallel}\sum_{\mathrm{p}} K_{\mathrm{p}}^2 + \chi_3^{\parallel}\sum_{\mathrm{t}} K_{\mathrm{t}}^2 + \chi_4^{\parallel}\sum_{\mathrm{c}} K_{\mathrm{c}}^2\right)\lambda_z^2 \\ &-\frac{1}{2\beta}\left(\chi_1^{\perp}\sum_{\mathrm{i}} K_{\mathrm{i}}^2 + \chi_2^{\perp}\sum_{\mathrm{p}} K_{\mathrm{p}}^2 + \chi_3^{\perp}\sum_{\mathrm{t}} K_{\mathrm{t}}^2 + \chi_4^{\perp}\sum_{\mathrm{c}} K_{\mathrm{c}}^2\right) \\ &\times(\lambda_x^2 + \lambda_y^2)\Bigg] \end{aligned} \tag{2.34}$$

where

$$\tilde{Z}_0 = \mathrm{Tr}[\exp(-\beta\tilde{H}_0)] \tag{2.35}$$

and

$$\langle \ldots \rangle_0 = \mathrm{Tr}[\ldots \exp(-\beta\tilde{H}_0)]/\tilde{Z}_0. \tag{2.36}$$

$\chi_1^{\parallel}, \ldots, \chi_4^{\parallel}$ and $\chi_1^{\perp}, \ldots, \chi_4^{\perp}$ are defined as

$$\chi_1^{\parallel} = \beta\frac{\partial}{\partial y}\langle S_{\mathrm{i}}^z\rangle_0 \qquad \chi_2^{\parallel} = \beta\frac{\partial}{\partial y}\langle S_{\mathrm{p}}^z\rangle_0 \qquad \chi_3^{\parallel} = \beta\frac{\partial}{\partial y}\langle S_{\mathrm{t}}^z\rangle_0 \qquad \chi_4^{\parallel} = \beta\frac{\partial}{\partial y}\langle S_{\mathrm{c}}^z\rangle_0$$

$$\chi_1^{\perp} = \beta\langle S_{\mathrm{i}}^z\rangle_0/y \qquad \chi_2^{\perp} = \beta\langle S_{\mathrm{p}}^z\rangle_0/y \qquad \chi_3^{\perp} = \beta\langle S_{\mathrm{t}}^z\rangle_0/y \qquad \chi_4^{\perp} = \beta\langle S_{\mathrm{c}}^z\rangle_0/y$$

where $y = \beta g_{\mathrm{Mn}}\mu_{\mathrm{B}}B_0$.

$(g_{\mathrm{Mn}}\mu_{\mathrm{B}})^2\chi^{\parallel}$ and $(g_{\mathrm{Mn}}\mu_{\mathrm{B}})^2\chi^{\perp}$ are, respectively, the longitudinal and transverse susceptibilities of the different clusters.

Substituting (2.34) into (2.23) and integrating over $\boldsymbol{\lambda}$ yields

$$\tilde{Z}_{\mathrm{BMP}} = C\int_{-\infty}^{\infty}\mathrm{d}\boldsymbol{\Delta}\exp(-\beta H_{\mathrm{eff}}(\boldsymbol{\Delta})) \tag{2.37}$$

where

$$C = \tilde{Z}_0(\beta/8\pi)^{3/2}(\varepsilon_{\mathrm{p}}^{\parallel}\varepsilon_{\mathrm{p}}^{\perp 2})^{-1/2}. \tag{2.38}$$

The effective spin Hamiltonian has the form

$$H_{\text{eff}}(\boldsymbol{\Delta}) = (1/\beta)\ln(f(\beta\Delta)) + (\Delta_x^2 + \Delta_y^2)/8\varepsilon_p^{+} + (\Delta_z - \Delta_0)^2/8\varepsilon_p^{\parallel}. \tag{2.39}$$

Δ can be shown to be related to the spin-flip Raman shift, and

$$\Delta_0 = g^*\mu_B B_0 + \langle S_i^z\rangle_0 \sum_i K_i + \langle S_p^z\rangle_0 \sum_p K_p + \langle S_t^z\rangle_0 \sum_t K_t + \langle S_c^z\rangle_0 \sum_c K_c \tag{2.40}$$

is the magnetic field induced spin-flip Raman shift. The characteristic energies of the BMP, $\varepsilon_p^{\parallel}$ and ε_p^{+}, are defined as

$$\varepsilon_p^{\parallel} = \frac{1}{4}\left(\chi_1^{\parallel}\sum_i K_i^2 + \chi_2^{\parallel}\sum_p K_p^2 + \chi_3^{\parallel}\sum_t K_t^2 + \chi_4^{\parallel}\sum_c K_c^2\right) \tag{2.41a}$$

$$\varepsilon_p^{+} = \frac{1}{4}\left(\chi_1^{+}\sum_i K_i^2 + \chi_2^{+}\sum_p K_p^2 + \chi_3^{+}\sum_t K_t^2 + \chi_4^{+}\sum_c K_c^2\right). \tag{2.41b}$$

To perform a configurational average over the Mn^{2+} impurities we make use of the continuum approximation, and use the wavefunction (2.2) in order to derive

$$\begin{aligned} &\sum_i K_i = JN_0xP_1 \qquad \sum_p K_p = JN_0xP_2 \\ &\sum_t K_t = JN_0xP_3 \qquad \sum_c K_c = JN_0xP_4 \end{aligned} \tag{2.42}$$

$$\begin{aligned} &\sum_i K_i^2 = \frac{J^2N_0xP_1}{8\pi a_B^3} \qquad \sum_p K_p^2 = \frac{J^2N_0xP_2}{8\pi a_B^3} \\ &\sum_t K_t^2 = \frac{J^2N_0xP_3}{8\pi a_B^3} \qquad \sum_c K_c^2 = \frac{J^2N_0xP_4}{8\pi a_B^3} \end{aligned} \tag{2.43}$$

where x is the concentration of Mn^{2+} ions, N_0 the number of cations per unit volume. P_1 is the probability of having an isolated Mn^{2+}, P_2 the probability of having a pair, P_3 the probability of having an open triangle, and P_4 the probability of having a closed triangle of Mn^{2+} ions. The cluster probabilities are given in Appendix 2. With the use of (2.42) and (2.43) Δ_0, $\varepsilon_p^{\parallel}$ and ε_p^{+} can be written as

$$\Delta_0 = g^*\mu_B B_0 + JN_0x(P_1\langle S_i^z\rangle_0 + P_2\langle s_p^z\rangle_0 + P_3\langle S_t^z\rangle_0 + P_4\langle S_c^z\rangle_0) \tag{2.44}$$

$$\varepsilon_p^{\parallel} = [(JN_0)^2x/32\pi a_B^3N_0](P_1\chi_1^{\parallel} + P_2\chi_2^{\parallel} + P_3\chi_3^{\parallel} + P_4\chi_4^{\parallel}) \tag{2.45}$$

$$\varepsilon_p^{+} = [(JN_0)^2x/32\pi a_B^3N_0](P_1\chi_1^{+} + P_2\chi_2^{+} + P_3\chi_3^{+} + P_4\chi_4^{+}). \tag{2.46}$$

The effective spin Hamiltonian (2.39) has the same form as the Hamiltonian of Dietl and Spalek [9, 10] and Dietl [11], who used the Gaussian approximation to the spin fluctuations within the Ginzburg–Landau theory. However their Hamiltonian contains the magnetic-field-induced macroscopic magnetisation which is introduced phenomenologically in the Ginzburg–Landau free-energy functional. In our derivation we included the Mn–Mn interaction microscopically in the form of small clusters. Hence the Hamiltonian obtained in this way contains microscopic expressions for the magnetisation of the different clusters. In addition, the work of Swierkowski and Dietl [12] has gone beyond the Gaussian approximation. It should be noted that the case of zero magnetic field and no Mn–Mn interaction can be solved exactly at the level of static approximation [14].

3. Spin-flip Raman scattering spectrum

With the simplified situation that during the spin-flip scattering the spins of all Mn^{2+} ions remain intact, the spin-flip spectrum can be calculated from the Fourier transform [24]

$$S(\omega) = \frac{1}{2\pi}\int_{-\infty}^{\infty} S(t)\,e^{i\omega t}\,dt \tag{3.1}$$

of the electron (or hole) spin–spin correlation function

$$S(t) = \langle [e^{iHt}\boldsymbol{s}\,e^{-iHt})\cdot\boldsymbol{\alpha}](\boldsymbol{s}\cdot\boldsymbol{\alpha})\rangle \tag{3.2}$$

where the Hamiltonian H is given by (2.4). The unit vector $\boldsymbol{\alpha}$ is determined by the geometry of the Raman scattering experiment.

To derive the spin–spin correlation function we start from the finite-temperature spin–spin Green function

$$G(\tau) = \langle T_\tau[(e^{\tau H}\boldsymbol{s}^{-\tau H})\cdot\boldsymbol{\alpha}](\boldsymbol{s}\cdot\boldsymbol{\alpha}^*)\rangle \qquad 0 \leqslant \tau \leqslant \beta. \tag{3.3}$$

In the interaction representation, $G(\tau)$ has the form

$$G(\tau) = \langle T_\tau\{[(e^{\tau H_0}\boldsymbol{s}\,e^{-\tau H_0})\cdot\boldsymbol{\alpha}](\boldsymbol{s}\cdot\boldsymbol{\alpha}^*)\}W(\beta)\rangle_0 / \langle W(\beta)\rangle_0 \tag{3.4}$$

where

$$W(\beta) = T_\tau\left[\exp\left(-\int_0^\beta H_1(\tau)\,d\tau\right)\right]. \tag{3.5}$$

H_0, H_1 and $\langle\ldots\rangle_0$ are defined in the last section by (2.6), (2.7) and (2.15) respectively.

In order to calculate the Green function, the functional integral approach will be used, and after a derivation similar to that in the last section $G(\tau)$ is obtained as

$$\begin{aligned} G(\tau) = (Z_{\mathrm{BMP}})^{-1}\int \mathrm{D}\boldsymbol{x}\int \mathrm{D}\boldsymbol{y}\exp\left(-\frac{1}{\beta}\int_0^\beta (x^2(\tau)+y^2(\tau))\,d\tau\right) \\ \times \mathrm{Tr}\Big\{e^{-\beta H_0}T_\tau\{[(e^{\tau H_0}\boldsymbol{s}\,e^{-\tau H_0})\cdot\boldsymbol{\alpha}](\boldsymbol{s}\cdot\boldsymbol{\alpha}^*)\} \\ \times \exp\left[\left(\frac{1}{\beta}\right)^{1/2}\int_0^\beta [\boldsymbol{\Gamma}(\tau)\cdot(\boldsymbol{x}(\tau)+i\boldsymbol{y}(\tau)) \right. \\ \left. + \boldsymbol{s}(\tau)\cdot(\boldsymbol{x}(\tau)-i\boldsymbol{y}(\tau))]\,d\tau\right]\Big\}. \end{aligned} \tag{3.6}$$

Within the static approximation, we have

$$\begin{aligned} G_{\mathrm{st}}(\tau) = (\pi^3\tilde{Z}_{\mathrm{BMP}})^{-1}\int_{-\infty}^{\infty} d\boldsymbol{x}_0\int_{-\infty}^{\infty} d\boldsymbol{y}_0\exp(-x_0^2-y_0^2) \\ \times \mathrm{Tr}[\![exp(-\beta H_{\mathrm{st}})T_\tau\{[(e^{\tau H_{\mathrm{st}}}\boldsymbol{s}\,e^{-\tau H_{\mathrm{st}}})\cdot\boldsymbol{\alpha}](\boldsymbol{s}\cdot\boldsymbol{\alpha}^*)\}]\!]. \end{aligned} \tag{3.7}$$

Substituting in H_{st} from (2.17) into (3.7) and changing the variables from $\boldsymbol{x}_0$ and $\boldsymbol{y}_0$ to $\boldsymbol{\lambda}$ and $\boldsymbol{\Delta}$, we have the form

$$G_{\mathrm{st}}(\tau) = (8\pi^3\tilde{Z}_{\mathrm{st}})^{-1}\int_{-\infty}^{\infty} d\boldsymbol{\Delta}\int_{-\infty}^{\infty} d\boldsymbol{\lambda}\exp[i\boldsymbol{\lambda}\cdot(\boldsymbol{\Delta}-\boldsymbol{b}_1)]Z_{\mathrm{Mn}}G(\tau,\boldsymbol{\Delta}) \tag{3.8}$$

where Z_{Mn} is given by (2.26), and

$$G(\tau, \boldsymbol{\Delta}) = \mathrm{Tr}_{\{s\}}\{\exp(\beta s \cdot \boldsymbol{\Delta}) T_\tau [(s(\tau) \cdot \boldsymbol{\alpha})(s \cdot \boldsymbol{\alpha}^*)]\} \tag{3.9}$$

with $s(\tau)$ defined as

$$s(\tau) = \exp(-\tau s \cdot \boldsymbol{\Delta}) s \exp(\tau s \cdot \boldsymbol{\Delta}). \tag{3.10}$$

The above equations are valid for any value of the spin s. So far, spin-flip Raman scattering has only been observed for a donor BMP. We will therefore consider the case spin $\frac{1}{2}$. $G(\tau, \boldsymbol{\Delta})$ is then calculated to be

$$G(\tau, \boldsymbol{\Delta}) = A(\boldsymbol{\Delta}) + B_+(\boldsymbol{\Delta})\, \mathrm{e}^{-\tau\Delta}(\mathrm{e}^{\beta\Delta/2}\Theta(\tau) + \mathrm{e}^{-\beta\Delta/2}\Theta(-\tau))$$
$$\times B_-(\boldsymbol{\Delta})\, \mathrm{e}^{\tau\Delta}(\mathrm{e}^{-\beta\Delta/2}\Theta(\tau) + \mathrm{e}^{\beta\Delta/2}\Theta(-\tau)) \tag{3.11}$$

where $\Theta(\tau)$ is the Heaviside step function and

$$A(\boldsymbol{\Delta}) = \tfrac{1}{2}(\boldsymbol{\Delta} \cdot \boldsymbol{\alpha})(\boldsymbol{\Delta} \cdot \boldsymbol{\alpha}^*) \cosh(\beta\Delta/2) \tag{3.12}$$

$$B_\pm(\boldsymbol{\Delta}) = \tfrac{1}{4}[\boldsymbol{\alpha} \cdot \boldsymbol{\alpha}^* - \Delta^{-2}(\boldsymbol{\Delta} \cdot \boldsymbol{\alpha})(\boldsymbol{\Delta} \cdot \boldsymbol{\alpha}^*) \pm \mathrm{i}\Delta^{-1}(\boldsymbol{\alpha} \times \boldsymbol{\alpha}^*) \cdot \boldsymbol{\Delta}]. \tag{3.13}$$

For each Matsubara frequency $\omega_n = (2\pi/\beta)n$ with $n = 0, \pm 1, \pm 2, \ldots$, we take the Fourier transform of $G(\tau, \boldsymbol{\Delta})$

$$G(\mathrm{i}\omega_n, \boldsymbol{\Delta}) = \frac{1}{\beta}\int_0^\beta G(\tau, \boldsymbol{\Delta}) \exp(\mathrm{i}\omega_n \tau)\, \mathrm{d}\tau = A(\boldsymbol{\Delta})\delta_{\omega_n, 0}$$
$$- \frac{2}{\beta} B_+(\boldsymbol{\Delta}) \frac{\sinh(\frac{1}{2}\beta\Delta)}{\mathrm{i}\omega_n - \Delta} + \frac{2}{\beta} B_-(\boldsymbol{\Delta}) \frac{\sinh(\frac{1}{2}\beta\Delta)}{\mathrm{i}\omega_n + \Delta}. \tag{3.14}$$

Making use of (3.14), the Fourier transform $G_{st}(\mathrm{i}\omega_n)$ of $G_{st}(\tau)$ is derived.

By performing the analytical continuation to real frequencies $\mathrm{i}\omega_n \to \omega + \mathrm{i}\eta$ ($\eta = 0^+$), we obtain the fourier transform $G_R(\omega)$ of the retarded Green function

$$G_R(t) = -\mathrm{i}\Theta(t)\langle[(\mathrm{e}^{\mathrm{i}Ht} s\, \mathrm{e}^{-\mathrm{i}Ht}) \cdot \boldsymbol{\alpha}, s \cdot \boldsymbol{\alpha}^*]\rangle$$

in the static approximation as [20]

$$G_R(\omega) = -(\beta/2\pi)\, G_{st}(\mathrm{i}\omega_n \to \omega + \mathrm{i}\eta). \tag{3.15}$$

Using the well established relation [25]

$$\mathrm{Im}\, G_R(\omega) = -\tfrac{1}{2}(1 - \mathrm{e}^{-\beta\omega}) S(\omega) \tag{3.16}$$

where $S(\omega)$ has been defined by (3.1), we have

$$S(\omega) = (8\pi^3 \tilde{Z}_{BMP})^{-1} \int_{-\infty}^{\infty} \mathrm{d}\boldsymbol{\Delta} \int_{-\infty}^{\infty} \mathrm{d}\boldsymbol{\lambda} \exp[\mathrm{i}\boldsymbol{\lambda} \cdot (\boldsymbol{\Delta} - \boldsymbol{b}_1)] Z_{Mn}$$
$$\times (A(\boldsymbol{\Delta})\delta(\omega) + B_+(\boldsymbol{\Delta})\mathrm{e}^{\beta\omega/2}\delta(\omega - \Delta) + B_-(\boldsymbol{\Delta})\mathrm{e}^{\beta\omega/2}\delta(\omega + \Delta)). \tag{3.17}$$

The three terms in the right-hand side with frequencies $\delta(\omega)$, $\delta(\omega - \Delta)$ and $\delta(\omega + \Delta)$ respectively correspond to the Faraday rotation, the Stokes shift and the anti-Stokes shift.

Since we are interested in the spin-flip Raman scattering, we will neglect the Faraday rotation term. If we use the cumulant expansion, as in the previous section, to calculate

Z_{Mn}, and then integrate over $\boldsymbol{\lambda}$, we obtain the final form

$$S(\omega) = \frac{C}{\tilde{Z}_{BMP}} \int_{-\infty}^{\infty} d\boldsymbol{\Delta} \exp\left(-\frac{\beta}{8}(\Delta_x^2 + \Delta_y^2)/\varepsilon_p^{\perp} - \frac{\beta}{8}(\Delta_z - \Delta_0)^2/\varepsilon_p^{\parallel} \right)$$

$$\times \left(B_+(\boldsymbol{\Delta})\, e^{\beta\omega/2}\delta(\omega - \Delta) + B_-(\boldsymbol{\Delta})\, e^{\beta\omega/2}\delta(\omega + \Delta) \right) \tag{3.18}$$

where C, Δ_0, $\varepsilon_p^{\parallel}$ and $\varepsilon_p^{\perp}$ are given by (2.38), and (2.44)–(2.46).

In the case of zero external magnetic field, $S(\omega)$ can be solved exactly as

$$S_0(\omega) \propto \omega^2\, e^{\beta\omega/2} \exp(-\tfrac{1}{8}\beta\omega^2/\varepsilon_p) \tag{3.19}$$

where

$$\varepsilon_p = [(JN_0)^2 x/32\pi a_B^3 N_0](P_1\chi_1 + P_2\chi_2 + P_3\chi_3 + P_4\chi_4) \tag{3.20}$$

and $(\mu_B g_{Mn})^2\chi$ is just the zero-magnetic-field susceptibility of the different clusters.

At the limit of high magnetic field, when most of the electrons have their quantisation axis $\boldsymbol{\Delta}/\Delta$ along the direction of the magnetic field, we can replace $\boldsymbol{\Delta}/\Delta$ in (3.13) with its component along the field. If we also neglect the anisotropy by setting $\varepsilon_p^{\perp} = \varepsilon_p^{\parallel} = \varepsilon_p$, equation (3.18) can again be solved to give

$$S(\omega) = (4\varepsilon_p/\beta\Delta_0\omega) \sinh(\beta\Delta_0\omega/4\varepsilon_p) S_0(\omega). \tag{3.21}$$

This result approaches $S_0(\omega)$ as B_0 goes to zero and can be used as a good approximation over the whole field range. Within the theory of Dietl and Spalek [9, 10], Dietl [11] has neglected anisotropy to calculate $S(\omega)$ without the above high-field approximation. Our results (3.19) and (3.21) agree with those obtained by Dietl [11] in the appropriate limit, except as regards the different ways we include the Mn–Mn interaction. If we neglect the Mn–Mn interaction, our results (3.19) and (3.21) agree with those obtained by Heiman and co-workers [7].

4. Calculations and results

4.1. Spin-flip Raman scattering for a donor BMP

From (3.21) it can be shown that the peak position, $\tilde{\omega}$, of the Stokes Raman line satisfies

$$\tilde{\omega}^2 - 2\varepsilon_p\tilde{\omega} - \tilde{\omega}\Delta_0 \coth(\beta\Delta_0\tilde{\omega}/4\varepsilon_p) - 4\varepsilon_p k_B T = 0. \tag{4.1}$$

The traces are calculated using the eigenvalues in Appendix 1. The effective Bohr radius a_B is determined from minimising the free energy with respect to a_B, and the change in the Bohr radius is found to be less than 2%. We will therefore use the Bohr radius for $x = 0$. Concerning the cluster probabilities, we would like to determine them using magnetisation data from the same samples on which spin-flip Raman scattering was measured. However, since we have not found such measurements we will use probabilities corresponding to a random distribution of Mn^{2+} ions, given in Appendix 2, and if necessary adjust the cluster probabilities. The cluster probabilities

Table 1. The cluster probabilities and the parameter T_0 used for the theoretical fits. The values corresponding to a random distribution (see Appendix 2) are written in parentheses.

	$Cd_{1-x}Mn_xSe$		$Cd_{1-x}Mn_xTe$	
	$x = 0.012$	$x = 0.051$	$x = 0.035$	$x = 0.044$
P_1	0.86	0.53	0.65	0.58
	(0.68)	(0.52)	(0.65)	(0.58)
P_2	0.058	0.12	0.11	0.12
	(0.11)	(0.12)	(0.11)	(0.12)
P_3	0.0045	0.032	0.022	0.02
	(0.019)	(0.033)	(0.022)	(0.02)
P_4	0.0019	0.044	0.02	0.033
	(0.016)	(0.049)	(0.02)	(0.033)
T_0 (K)	0.4	1.6	1.4	2.4

Table 2. Material parameters used in the calculations.

Quantity	Symbol	$Cd_{1-x}Mn_xSe$	$Cd_{1-x}Mn_xTe$
Intrinsic g-factor[a]	g^*	0.52	−0.75
Nearest-neighbour Mn–Mn exchange constant (K)[b]	I	−8.3	−6.9
Intrinsic Bohr radius (Å)[c]	a_B	38	52.4
s–d exchange constant (eV)[d]	αN_0	0.261 ± 0.013	0.22 ± 0.01

[a] For the $x = 0$ alloy, from [27].
[b] From [28] and [29].
[c] For the $x = 0$ alloy. The Bohr radius was calculated from the effective mass $m^*/m_0 = 0.13$ and the dielectric constant $\kappa = 9.4$ for $Cd_{1-x}Mn_xSe$ [30]. For $Cd_{1-x}Mn_xTe$, $m^*/m_0 = 0.11$ and $\kappa = 10.9$ [8].
[d] From [26] and [31].

used in the calculations are given in table 1. Other parameter values used in the calculations are given in table 2.

The spin-flip Raman shift for $Cd_{1-x}Mn_xSe$ with $x = 0.012$ is plotted in figure 1 (full and broken curves), as a function of magnetic field at various temperatures. The corresponding experimental data are indicated with full circles. In comparison with experimental data, the broken curve saturates too fast. This kind of behaviour was first observed by Gaj and co-workers [26] in another situation, namely when they tried to fit the Brillouin function to magnetisation data on $Cd_{1-x}Mn_xTe$. They found that the data could be fitted better, if the adjustable parameter T_0 is introduced by replacing T, in the argument of the Brillouin function, by $T + T_0$. This empirical procedure is supposed to take into account a weak long-range antiferromagnetic Mn–Mn interaction. Since we have included only nearest-neighbour interaction, we follow the argument of [26], and write the magnetisation and the susceptibility for an isolated

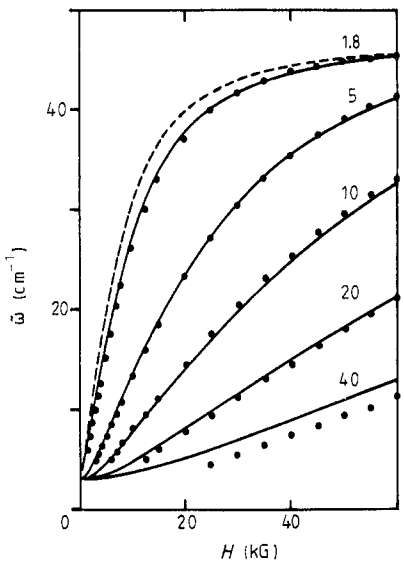

Figure 1. The magnetic field and temperature dependence of the peak spin-flap Raman shift in $Cd_{1-x}Mn_xSe$, $x = 0.012$. The curves are generated from (4.1), and the full circles are experimental data from [8]. See tables 1 and 2 for parameters. Note that the broken curve was generated with $T_0 = 0$. The values on the curves are in K.

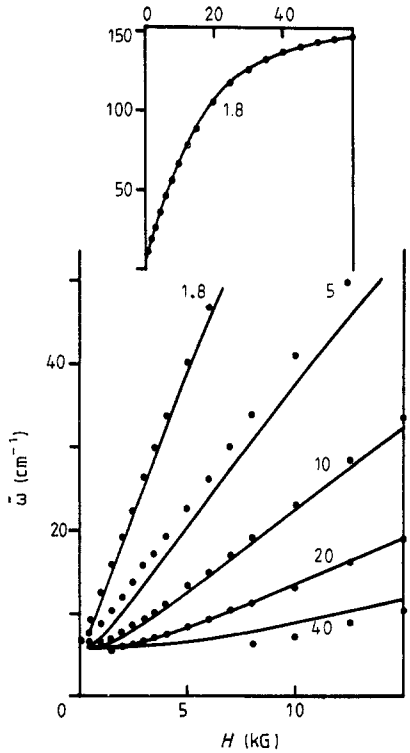

Figure 2. The magnetic field and temperature dependence of the peak spin-flip Raman shift in $Cd_{1-x}Mn_xSe$, $x = 0.051$. The curves are generated from (4.1), and the full circles are experimental data from [8]. See tables 1 and 2 for parameters. The values on the curves are in K.

Mn^{2+} ion as

$$\langle S_j^z \rangle_0 = \tfrac{5}{2} B_{5/2}(\bar{y}) \tag{4.2}$$

$$\chi_1 = [1/k_B(T + T_0)](\partial/\partial y)\langle S_j^z \rangle_0 |_{y=\bar{y}} \tag{4.3}$$

where $\bar{y} = \mu_B g_{Mn} B_0 / k_B(T + T_0)$. T_0 is given in table 1 for the best theoretical fits.

The theoretical curves for $Cd_{1-x}Mn_xSe$ with $x = 0.012$, after introducing T_0, are shown in figure 1 as full curves. Figure 2 shows similar results for $Cd_{1-x}Mn_xSe$ with $x = 0.051$. For $Cd_{1-x}Mn_xTe$ with $x = 0.035$ and $x = 0.044$, the theoretical results are shown, respectively, in figures 3 and 4 (as full curves) together with experimental data (as full circles).

Other than for $Cd_{1-x}Mn_xSe$ with $x = 0.012$, our computed results using a random distribution of Mn^{2+} ions agree well with experiments. However, for $Cd_{1-x}Mn_xSe$ with $x = 0.012$, we must use cluster probabilities corresponding to a stronger clustering of Mn^{2+} ions. We notice that for both $Cd_{1-x}Mn_xSe$ and $Cd_{1-x}Mn_xTe$ at higher Mn^{2+}

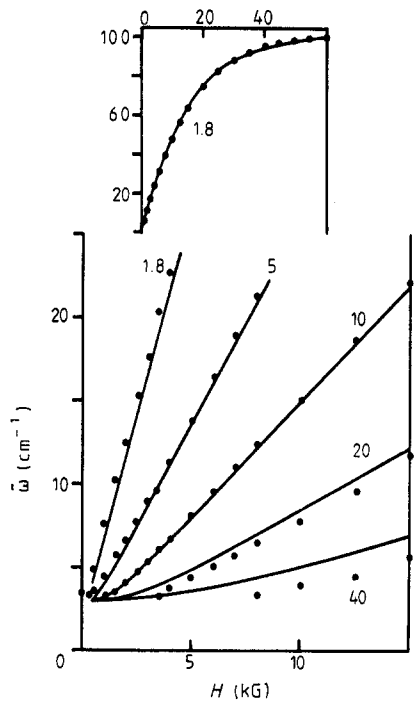

Figure 3. The magnetic field and temperature dependence of the peak spin-flip Raman shift in $Cd_{1-x}Mn_xTe$, $x = 0.035$. The curves are generated from (4.1), and the full circles are experimental data from [8]. See tables 1 and 2 for parameters. The values on the curves are in K.

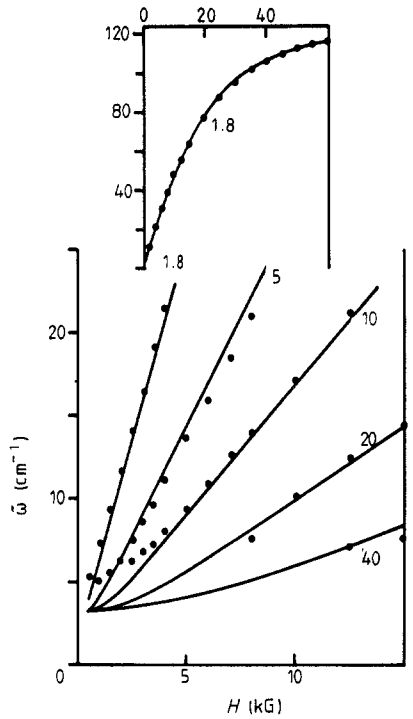

Figure 4. The magnetic field and temperature dependence of the peak spin-flip Raman shift in $Cd_{1-x}Mn_xTe$, $x = 0.044$. The curves are generated from (4.1), and the full circles are experimental data from [8]. See tables 1 and 2 for parameters. The values on the curves are in K.

concentration, figures 3 and 4 show increasing discrepancy between theoretical curves and experimental values as the magnetic field gets weaker. A better fit for low magnetic field can be obtained by adjusting the Bohr radius, which has been done by Peterson and co-workers [8] when they fitted the theory of Dietl and Spalek [9, 10] to their experimental data. This is not unreasonable since the Bohr radius depends on the effective mass and the static dielectric constant, which can both depend on composition.

4.2. Binding energy for an acceptor BMP

For an acceptor BMP in p-$Cd_{1-x}Mn_xTe$, with a small Bohr radius ($a_B \simeq 13$ Å), the cumulant expansion and the continuum approximation in § 2 are not accurate at low temperatures. Hence we expect an increasing deviation of the calculated binding energy from the measured value. We write the binding energy for an acceptor BMP as

$$E = h^2/2m^*a_B^2 - e^2/\varepsilon a_B - \partial \ln(Z_{BMP})/\partial\beta. \tag{4.4}$$

In the case of zero magnetic field, using (2.35), (2.37)–(2.39), we have

$$\tilde{Z}_{BMP} = 2\tilde{Z}_0[(1 + \beta\varepsilon)\, e^{\beta\varepsilon_p/2} + (1 + 9\beta\varepsilon_p)\, e^{9\beta\varepsilon_p/2}] \tag{4.5}$$

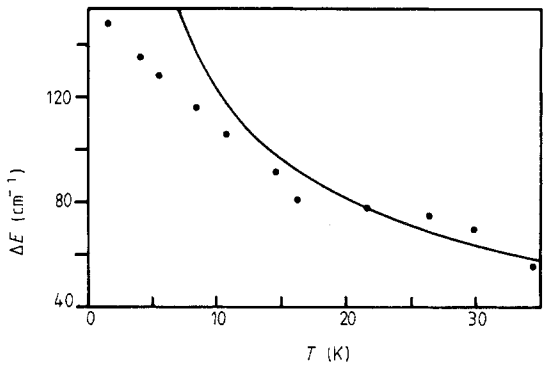

Figure 5. The magnetic part of the binding energy, calculated from the magnetic part of (4.6), for p-$Cd_{1-x}Mn_xTe$, $x = 0.05$. The full circles are experimental data from [3].

where ε_p is given by (3.20). The term $-\partial \ln(\tilde{Z}_0)/\partial\beta$ will be subtracted since it is not relevant to us. Then the binding energy is

$$E = \frac{\hbar^2}{2m^* a_B^2} - \frac{e^2}{\varepsilon a_B} - \left(\varepsilon_p + \beta\frac{\partial \varepsilon_p}{\partial \beta}\right)\left(\frac{\frac{3}{2} + \frac{1}{2}\beta\varepsilon_p + 9\,e^{4\beta\varepsilon_p} + \frac{9}{2}(1+9\beta\varepsilon_p)\,e^{4\beta\varepsilon_p}}{1+\beta\varepsilon_p + (1+9\beta\varepsilon_p)\,e^{4\beta\varepsilon_p}}\right). \tag{4.6}$$

Since we have not taken the complex form of the hole wavefunction into account we follow the procedure of Jaroszynski and co-workers [32]: we replace the exchange integral βN_0 by $0.8\beta N_0$, where $\beta N_0 = -0.88$ eV [26]. For a given value of x, the Bohr radius a_B should be determined from minimisation of the free energy with respect to a_B. But in view of the approximations already performed we will not take the exchange-induced change in the Bohr radius into account. The Bohr radius for $x = 0$ is $a_B = 13$ Å [14]. The cluster probabilities are calculated for a random distribution (see Appendix 2), and they are $P_1 = 0.54$, $P_2 = 0.119$, $P_3 = 0.03$, and $P_4 = 0.043$. The nearest-neighbour exchange integral is $I = -6.9$ K [29], and the parameter T_0 is chosen as $T_0 = 2.4$ K. In figure 5 we show the magnetic part ΔE of the binding energy for $Cd_{1-x}Mn_xTe$ with $x = 0.05$. The theoretical curve is calculated from the magnetic part of (4.6), and the experimental data are taken from [3].

5. Final remarks

We have analysed the recent theories of BMPs in diluted magnetic semiconductors by using the functional integral method. We have shown that existing theories are on the level of the static approximation, so to a certain extent they neglect the quantum fluctuations. We have included the antiferromagnetic interaction between the Mn^{2+} ions, in terms of small clusters with nearest-neighbour interactions. Comparison with experiments shows that in order to fit the theory qualitatively to experimental data, it is not necessary to take the nearest-neighbour Mn–Mn interaction into account in an exact form. One can make a good fit by phenomenologically introducing an effective concentration. We had to take into account the Mn–Mn interaction between more distant Mn^{2+} ions, by introducing a phenomenological parameter T_0. It is still a challenging theoretical problem to include the Mn–Mn interaction between more distant neighbours.

In order to test existing theories in more detail, it would be good to have detailed spin-flip Raman scattering measurements, as a function of magnetic field and temperature for various concentrations, where the magnetisation had also been measured on the same samples. Since there now exist measurements on BMPs in the millikelvin range of temperatures, it would be an interesting problem to include quantum corrections to the existing theories. Another area where there is need for more theoretical work is the dynamics of BMP formation where, lately, a lot of related experiments have been undertaken.

Acknowledgments

We would like to thank Dr T Dietl for stimulating discussions. This work was financially supported by the Swedish Natural Science Research Council under Grant No NFR-FFU-3996-127.

Appendix 1

The eigenvalues of (2.30*a*)–(2.30*d*) are:

$$E_i^0 = -b_2 m \qquad |m| \leqslant \tfrac{5}{2}$$

$$E_p^0 = -b_2 m - I[S(S+1) - \tfrac{35}{2}] \qquad 0 \leqslant S \leqslant 5, |m| \leqslant S$$

$$E_t^0 = -b_2 m - I[S(S+1) - S_a(S_a+1) - \tfrac{35}{4}] \qquad 0 \leqslant S_a \leqslant 5, |S_a - \tfrac{5}{2}| \leqslant S \leqslant S_a + \tfrac{5}{2}, \; |m| \leqslant S$$

$$E_c^0 = -b_2 m - I[S(S+1) - \tfrac{105}{4}] \qquad 0 \leqslant S_a \leqslant 5, |S_a - \tfrac{5}{2}| \leqslant S \leqslant S_a + \tfrac{5}{2}, \; |m| \leqslant S.$$

Appendix 2

In zincblende $A^{II}_{1-x}Mn_xB^{VI}$ alloys the Mn^{2+} ions occupy a FCC sublattice. Assuming a random distribution we have for the cluster probabilities

$$P_1 = (1-x)^{12} \qquad P_3 = 6x^2(1-x)^{23}(7-5x)$$

$$P_2 = 6x(1-x)^{18} \qquad P_4 = 8x^2(1-x)^{22}.$$

Since the cluster probabilities should satisfy, $P_1 + 2P_2 + 3P_3 + 3P_4 = 1$, P_4 can be calculated as

$$P_4 = \tfrac{1}{3}(1 - P_1 - 2P_2 - 3P_3).$$

In wurtzite alloys, where the Mn^{2+} ions occupy a HCP sublattice, the probabilities are the same except P_4, but the difference from the zincblende value is not significant for low concentrations of Mn^{2+} ions.

References

[1] Golnik A, Gaj J A, Nawrocki M, Planel M and Benoit â la Guillaume C 1980 *J. Phys. Soc. Japan Suppl.* A **49** 819
[2] Golnik A, Ginter J and Gaj J A 1973 *J. Phys. C: Solid State Phys.* **16** 6073
[3] Nhung T H, Planel R, Benoit â la Guillaume C and Bhattacharjee A K 1985 *Phys. Rev.* B **31** 2388
[4] Nawrocki M, Planel R, Fishman G and Galazka R R 1981 *Phys. Rev. Lett.* **46** 735
[5] Alov D L, Gubarev S I and Timofeev V B 1983 *Sov. Phys.–JETP* **57** 1052
[6] Alov D D, Gubarev S I, Timofeev V B and Shepel B N 1981 *JETP Lett.* **34** 71; 1984 *Sov. Phys.–JETP* **59** 658
[7] Heiman D, Wolff P A and Warnock J 1983 *Phys. Rev.* B **27** 4848
[8] Peterson D L, Bartholomew D U, Debska U, Ramdas A K and Rodriguez S 1985 *Phys. Rev.* B **32** 323
[9] Dietl T and Spalek J 1982 *Phys. Rev. Lett.* **48** 355
[10] Dietl T and Spalek J 1983 *Phys. Rev.* B **28** 1548
[11] Dietl T 1983 *J. Magn. Magn. Mater.* **38** 34
[12] Swierkowski L and Dietl T 1988 *Acta Phys. Polon.* A **73** 431
[13] Wolff P A and Warnock J 1984 *J. Appl. Phys.* **55** 2300
[14] Warnock J and Wolff P A 1985 *Phys. Rev.* B **31** 6579
[15] Ryabchenko S M and Semenov Yu G 1983 *Sov. Phys.–JETP* **57** 825
[16] Thibblin U, Chao K A and Micnas R 1986 *J. Phys. C: Solid State Phys.* **19** L303
[17] Golnik A and Spalek J 1986 *J. Magn. Magn. Mater.* **54–57** 1207
[18] Bhattacharjee A K 1986 *Solid State Commun.* **57** 31
[19] Micnas R, Thibblin U and Chao K A 1988 *Phys. Rev.* B **37** 4774
[20] Abrikosov A A, Gorkov L P and Dzyaloshinskii I E 1963 *Methods of Quantum Field Theory in Statistical Physics* (Englewood Cliffs, NJ: Prentice-Hall)
[21] Morandi G, Galleani d'Agliano E, Napoli F and Ratto C F 1974 *Adv. Phys.* **23** 867
[22] Muhlschlegel B 1978 *Path Integrals in Quantum and Statistical and Solid State Physics* ed. G J Papadopoulos and J T Devreese (New York: Plenum)
[23] Micnas R 1979 *Physica* A **98** 403
[24] Wolff P A, Ramos J C and Yuen S 1977 *Theory of Light Scattering in Condensed Matter* ed. B Bendow, J L Birman and V M Agranovich (New York: Plenum)
[25] Doniach S and Sondheimer E H 1974 *Green's Functions for Solid State Physicists* (Reading, MA: Benjamin)
[26] Gaj J A, Planel R and Fishman G 1979 *Solid State Commun.* **29** 435
[27] Walker T W, Litton C W, Reynolds D C, Collins T C, Wallace W A, Gorrell J H and Jungling K C *Proc. 11th Int. Conf. Physics of Semiconductors (Warszaw) 1972*
[28] Shapira Y, Foner S, Ridgley D H, Dwight K and Wold A 1984 *Phys. Rev.* B **30** 4021
[29] Spalek J, Lewicki A, Tarnawski Z, Furdyna J K, Galazka R R and Obuszko Z 1986 *Phys. Rev.* B **33** 3407
[30] Henry C, Nassau K and Shiever J W 1972 *Phys. Rev.* B **5** 458
Woodbury M H and Aven M 1974 *Phys. Rev.* B **9** 1595
[31] Shapira Y, Heiman D and Foner S 1982 *Solid State Commun.* **44** 1243
[32] Jaroszynski J, Dietl T, Sawicki M and Janik E 1983 *Physica* B **117+118** 473